Eur Biophys J (2001) 30: 330–343
DOI 10.1007/s002490100155

ARTICLE

Lukas D. Schuler · Peter Walde · P. Luigi Luisi
Wilfred F. van Gunsteren

Molecular dynamics simulation of *n*-dodecyl phosphate aggregate structures

Received: 4 January 2001 / Revised version: 19 March 2001 / Accepted: 20 March 2001 / Published online: 20 July 2001

Abstract Aggregates of *n*-dodecyl phosphate present an attractive model system of simple phospholipid amphiphile supramolecular structures for study by molecular dynamics simulation, since these systems have previously been studied experimentally under various conditions. A detailed molecular dynamics description of the properties of planar bilayer membranes (as a model for unilamellar vesicular membranes) and spherical micelles under various simulated conditions is presented. It is shown that the united-atom model of GROMOS96 applying the force-field parameter set 43A2 for biomolecular systems yields properties in agreement with experimental ones in most cases. Hydrogen bonding plays a role in stabilizing the bilayer aggregates at low pH, but not for the micelles, which are energetically favoured at high pH. NMR $-S_{CD}$ order parameters for a lipid bilayer system, the diffusion of amphiphiles within aggregates and of counterions, and lifetimes of hydrogen bonds between amphiphiles and to water are estimated from the MD simulations.

Keywords Dodecyl phosphate aggregates · Unilamellar bilayer membrane · Spherical micelle · GROMOS96 · Molecular dynamics simulation

Introduction

It has been suggested that simple phospholipids may have played an essential role in the prebiological, chemical evolution on Earth (Ourisson and Nakatani 1994, 1995; Deamer 1997; Luisi 1998; Luisi et al. 1999). Single-tail fatty acids (Boggs 1987; Walde et al. 1994; Morigaki et al. 1997; Blöchliger et al. 1998) and also alkyl phosphates or phosphonates were shown to vesiculate under conditions at which about one half of the molecules is negatively charged and the other half is uncharged. Between about pH 7–9 this is the case for fatty acids; around pH 2 it is the case for alkyl phosphates or phosphonates (Walde et al. 1997). Somewhat more complex phospholipids such as double-tail (Wagenaar et al. 1989; Buwalda et al. 1997) and cyclic (Buwalda et al. 1997) dialkyl or branched (Ravoo and Engberts 1994) monoalkyl phosphates have also been studied experimentally in this respect. A particular single-tail phospholipid, *n*-dodecyl phosphate, has been studied experimentally to some extent and was found to form both vesicles (at low pH) and micelles (at high pH), depending on the pH conditions of the aqueous solution (Tahara et al. 1969; Arakawa and Pethica 1980; Walde et al. 1997). If only unilamellar vesicles, which vary in diameter after spontaneous vesiculation, are considered, one roughly finds diameters in the range 25–250 nm. For the larger vesicles, a small patch of bilayer vesicular membrane shows negligible curvature. Undulations of membranes allow for locally convex or concave curvature (Zhang and Ouyang 1999). It is therefore reasonable to assume that a patch of vesicular membrane could be modelled to a good approximation as a planar bilayer patch. Experimentalists have indicated that hydrogen bonding may increase the stability of bilayers, which could explain vesicle formation at $pH \approx pK_1 = 2$ (Deamer 1997). For intermediate pH values of 7.5, for example, Walde et al. (1997) observed large insoluble aggregates for *n*-dodecyl phosphates. At $pH = 11.2$ the aggregates have completely disappeared, as inferred from light and electron microscopy, and micelles are assumed to exist in the case of single-tail lipids (Walde et al. 1997). Under salty conditions (0.5 M NaCl) the formation of micelles at high pH has been noted as well (Tahara et al. 1969; Arakawa and Pethica 1980). Apart from the sketched dependence of the aggregation state on pH, not much is known about *n*-dodecyl phosphate aggregates. No NMR order parameters of pure *n*-dodecyl phosphoric acid

L.D. Schuler · P. Walde · P.L. Luisi · W.F. van Gunsteren (✉)
Department of Chemistry, Swiss Federal Institute
of Technology Zürich, ETH-Zentrum,
8092 Zürich, Switzerland
E-mail: wfvgn@igc.phys.chem.ethz.ch

or its salts have been measured to our knowledge. The only X-ray examination we are aware of suggests that solubility and crystalline appearance are similar to fatty acids, and alkyl dihydrogen phosphates would show a tilting angle of 37° in the crystal form (Brown et al. 1955), which could also be relevant for a bilayer structure.

Molecular dynamics (MD) simulation offers the possibility to study the structural, dynamical and energetic properties of complex systems in atomic detail, provided a reliable force field is available and the conformational space of the system is sufficiently sampled (van Gunsteren and Berendsen 1990). Molecular systems containing lipids in various forms, liquid crystals, monolayers, bilayers and micelles, have been studied with MD simulation (Egberts and Berendsen 1988; Ahlström and Berendsen 1993; Damodaran and Merz 1994; Egberts et al. 1994; Yonega and Berendsen 1994; MacKerell 1995; Callaway et al. 1996; Tieleman and Berendsen 1996; Tobias and Klein 1996; Kuhn and Rehage 1997; Larson 1997; Tieleman et al. 1997; Essmann and Berkowitz 1999). Here we have used MD simulation on a nanosecond timescale to investigate systems built up from mixtures of *n*-dodecyl phosphates and *n*-dodecyl phosphoric acid under various conditions of pH and temperature, starting from bilayer and micellar structures. Although the simulation timescale is too short to observe transitions between the different types of lipid aggregates, analysis and comparison of the structural, dynamical and energetic differences between various simulations should give insight into the interactions that govern the association and structure of assemblies of single-chain phospholipids.

Methods

Molecular model and force field

The molecular systems were modelled using the GROMOS96 force field, which uses a united-atom representation for aliphatic hydrocarbons (van Gunsteren et al. 1996, 1998; Daura et al. 1998; Schuler and van Gunsteren 2000). Figure 1 shows the molecular topology and partial atomic charges of *n*-dodecyl phosphoric acid and the two *n*-dodecyl phosphates in the three charge states (neutral, $-e$, $-2e$) that were used in the simulations. To mimic the various pH conditions, we combined the acidic, monoanionic or dianionic forms with each other in various ratios. At $pK_1 \approx pH = 2$ we combine the acidic and monoanionic forms in a 1:1 ratio. At $pK_2 \approx pH = 7$ we have approximately a 1:1 ratio of the monoanionic and the dianionic forms. At basic $pH = 11.2$ we have only the dianionic forms. We assume that these compositions of the system reflect the pH-dependent differences for a real system, since standard classical molecular dynamics simulation does not include the transfer of protons. Water was modelled using the simple point charge (SPC) model (Berendsen et al. 1981). The quality of the results of classical MD simulation is determined largely by the empirical force field that is used. To provide detailed information on this, the structural elements of the phospholipids and their respective force-field parameters are listed in Table 1. The functional forms of the various bonded and non-bonded interaction terms have been given previously (van Gunsteren et al. 1996; Scott et al. 1999). The 1-4 interaction for aliphatic hydrocarbons has recently been modified to improve the *trans* to *gauche* ratio for liquid *n*-alkanes (Schuler and van Gunsteren 2000). This improved parameter set is indicated as GROMOS96 set 43A2.

In simulations of mixed *n*-dodecyl phosphoric acid and *n*-dodecyl phosphate bilayers based on parameter set 43A1, no

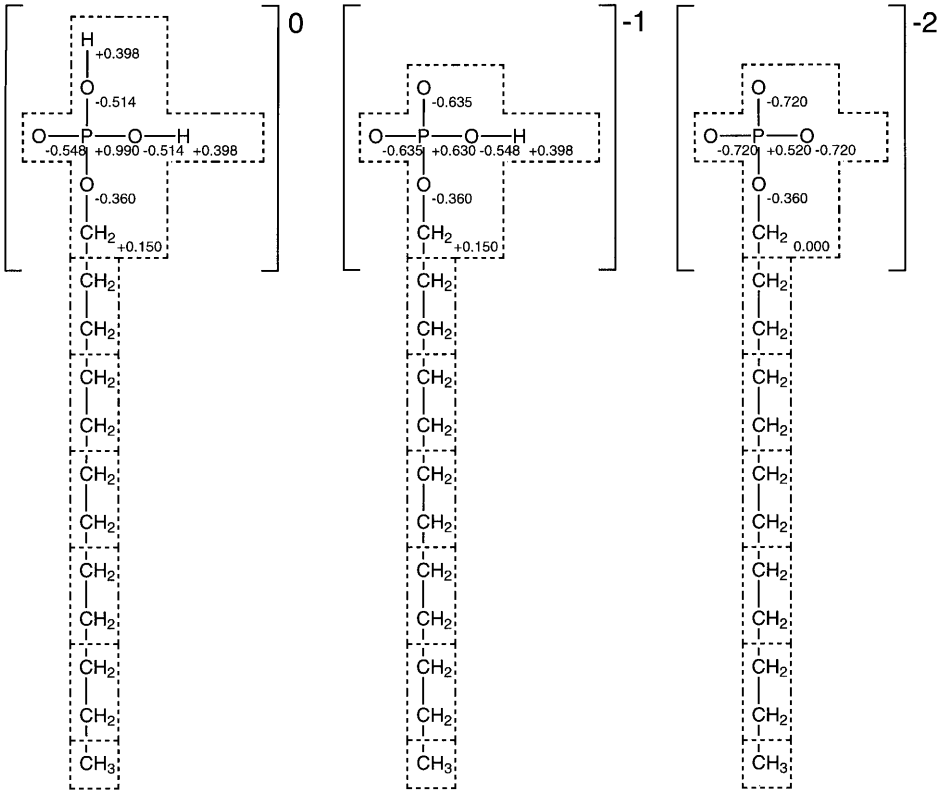

Fig. 1 Acidic, monoanionic and basic forms of *n*-dodecyl phosphate. The phosphate monoanion head group has been defined previously (van Gunsteren et al. 1996; see page IV-228) for use in 3-phospho-D-glycerate (PDG). GROMOS96 building block definitions include charge groups (indicated by *dashed boxes*) and partial charges (indicated by *real numbers*). Charges are given in *e* and have been chosen analogous to those of other phosphates. For aliphatic hydrocarbons (CH_n), united atoms are used. Note that they are not charged and therefore no charge has been displayed. For the definition of atom types, bond, bond-angle and dihedral-angle potential energy terms, see Table 1

Table 1 Structural elements and their respective force field parameters. On the left-hand side we show structural elements of *n*-dodecyl phosphates as contained in Fig. 1. We use "–" for bonds, "––" for bonds defining the bond and bond-angle types or for central bonds of torsional dihedral angle types and "∼" to indicate that there is possibly no bond but the end of a structural element. For atom types the GROMOS96 mass type code (MC) and integer atom code (IAC) are given in the second and third left column. Note that GROMOS96 (Scott et al. 1999) uses different $C_{12}^{1/2}(i)C_{12}^{1/2}(j)$ combinations for pairs (i,j) consisting of two polar atoms, consisting of a polar and a highly charged atom or consisting of oppositely charged atoms. These combinations are indicated by the respective structural elements under the corresponding $C_{12}^{1/2}$ values. Bond, bond-angle and torsional dihedral-angle types are for use with GROMOS96 potential energy terms for bonded interactions. The force field parameters have been taken from the set 43A2 (Schuler and van Gunsteren 2000). This set differs from the standard GROMOS96 43A1 set (Daura et al. 1998) with respect to dihedral-angle and third-neighbour non-bonded interaction parameters of *n*-alkane chains (bold italic numbers in the table)

Atom type	MC	IAC	Mass (a.m.u.)	$C6^{1/2}$ [(kJ mol^{-1} nm^{+6})$^{1/2}$]	$C12^{1/2}$ [10^{-3} (kJ mol^{-1} nm^{+12})$^{1/2}$]	$C12^{1/2}$ [10^{-3} (kJ mol^{-1} nm^{+12})$^{1/2}$]	$C12^{1/2}$ [10^{-3} (kJ mol^{-1} nm^{+12})$^{1/2}$]	$CS6^{1/2}$ [(kJ mol^{-1} nm^{+6})$^{1/2}$]	$CS12^{1/2}$ [10^{-3} (kJ mol^{-1} nm^{+12})$^{1/2}$]
–O	2	16	15.9994	0.04756	0.8611	1.841	3.068	0.04756	0.8611
				–O	–O–	P, Na+			
–O–	3	16	15.9994	0.04756	1.125	1.227	–	0.04756	1.1250
					–O, –O–, P, Na+				
$–CH_2–$	13	4	14.027	0.08429	5.077	–	–	0.06873	*2.1775964*
$–CH_3$	14	5	15.035	0.09958	5.794	–	–	0.08278	*2.4557820*
–H	18	1	1.008	0.0	0.0	–	–	0.0	0.0
–P–	27	31	30.9738	0.1214	4.711	–	–	0.1214	4.711

Bond type	Type code	K_{b_n} (10^6 kJ mol^{-1} nm^{-4})	Ideal bond length (nm)
–O––H	1	15.70	0.100
$–CH_2––O–$	17	8.18	0.143
–P––O	23	8.60	0.148
$\sim CH_n––CH_2–$	26	7.15	0.153
–P––O–	27	4.84	0.161

Bond angle type	Type code	K_{θ_n} (kJ mol^{-1})	Ideal bond angle (°)
$–CH_2–O––P––O–H$	4	420	103.0
–P––O––H	11	450	109.5
$–CH_2–O––P––O$	13	450	109.6
$\sim CH_n––CH_2––CH_2–$	14	530	111.0
$–CH_2––CH_2––O–$	14	530	111.0
$–CH_2––O––P–$	25	530	120.0
O––P––O	28	780	120.0

Torsional angle type	Type code	K_{φ_n} (kJ mol^{-1})	Phase	Multiplicity
$–CH_2–O––P–O\sim$	9	3.14	+1.0	2
$–CH_2–O––P–O\sim$	11	1.05	+1.0	3
$\sim O–P––O–H$	9	3.14	+1.0	2
$\sim O–P––O–H$	11	1.05	+1.0	3
$–CH_2–CH_2––O–P–$	14	3.77	+1.0	3
$–CH_2–CH_2––CH_2–O–$	17	***5.92***	+1.0	3
$\sim CH_n–CH_2––CH_2–CH_2–$	17	***5.92***	+1.0	3

transition of the bilayers from the starting all-*trans* conformations to a liquid-crystalline phase were observed (unpublished results). With the newer parameter set 43A2 (Schuler and van Gunsteren 2000) a complete melting of the membrane is observed if the temperature is raised sufficiently.

System set-up

Table 2 shows the different systems that were studied. A bilayer patch of twice 8×8 lipids (32 neutral ones and 32 with charge $-e$) was simulated with 64 Na^+ ions at $pK_1 \approx 2$ for three different temperatures, 298, 348 and 398 K. At basic pH the bilayer patch consists of twice 8×8 lipids with charge $-2e$, 256 Na^+ ions and many more water molecules. Three types of micellar systems were simulated. At $pK_1 \approx 2$ the system consists of 90 lipids with different tail lengths (45 neutral ones and 45 with charge $-e$) and 45 Na^+ ions and water. The one with the longer tails was simulated at $pK_2 \approx 7$ (45 lipids with charge $-e$ and 45 lipids with charge $-2e$) and at basic pH (90 lipids with charge $-2e$). Finally, a smaller micelle (64 lipids with charge $-2e$) was simulated at this pH. The number of 90 lipids was chosen as the average of the experimentally determined aggregation numbers (Tahara et al. 1969). We note that for the shorter tail length (C8) we would expect an aggregation number of 43 ± 5 at comparable conditions of pH = 4.5 and $T = 303$ K (Chevalier and Chachaty 1984).

For bilayers we used rectangular periodic boundary conditions, for micelles truncated octahedral ones. To obtain an initial structure for the bilayer patches an estimate of the head-group area of the lipids is useful. For *n*-dodecyl phosphate this quantity is actually not known experimentally. A rough estimate was obtained as follows. Aggregates of lipids may be characterized using a geometric packing parameter P (Israelachvili 1991). For example, a spherical micelle is characterized by $P < 1/3$, and a planar bilayer by $P = 1$. The area a_0 occupied by one head group is approximately given as a function of the carbon tail length l_c and the volume v of the carbon tail by:

$$a_0 = \frac{v}{l_c P} \tag{1}$$

For an elongated all-*trans* *n*-alkyl single chain with 12 carbons we assume that $l_c = 1.672$ nm and that $v = 0.3502$ nm^3 (Israelachvili 1991). For our bilayer patch ($P = 1$), assuming all-*trans* conformations, this leads to a value of $a_0 = 0.21$ nm^2.

At pK_1 the uncharged acid and the monoanion lipids are present in a 1:1 ratio positioned in a chess board-like geometry. This leads to a lipid-lipid neighbour to neighbour distance of 0.46 nm. For bilayers, the initial assembly of translated molecules was randomized with rotations of individual lipids around their body axis. Micelles were constructed by modifications of head groups and subsequently simulating the assembly of lipids while restraining their CH_3 tail atoms to a fixed position until the structure became spherical. Then the restraints were removed and solvent molecules as well as ions were added. Energy minimization was carried out followed by short (50 ps) MD simulation while restraining the positions of the lipid atoms.

Table 2 Simulated systems and their simulation conditions. The system labels are used throughout this work and the table is meant as a reference for the various simulation conditions. Five different groups of simulations can be distinguished: bilayers at low ($pK_1 = 2$) or high pH ($= 11.2$) and micelles at low (pK_1) or neutral (pK_2) and basic pH. Experiments (Walde et al. 1997) indicate the existence of bilayers at low and micelles at high pH

Parameter	Bilayer					
Label	bil-pK_1-298	bil-pK_1-348	bil-pK_1-398	bil-bas-298	bil-bas-348	bil-bas-398
Number of lipids	128	128	128	128	128	128
Number of tail carbons	12	12	12	12	12	12
Number of Na^+ ions	64	64	64	256	256	256
Number of water molecules	1420	1420	1420	7351	7351	7351
Atoms in total	6692	6692	6692	24,485	24,485	24,485
pH	p$K_1 \approx 2$	p$K_1 \approx 2$	p$K_1 \approx 2$	Basic	Basic	Basic
T (K)	298	348	398	298	348	398
Box shape	Rectangular	Rectangular	Rectangular	Rectangular	Rectangular	Rectangular
Pressure coupling	Anisotropic	Anisotropic	Anisotropic	Anisotropic	Anisotropic	Anisotropic
Initial box lengths						
x (nm)	3.68	3.68	3.68	3.80	3.80	3.80
y (nm)	3.68	3.68	3.68	3.50	3.50	3.50
z (nm)	7.60	7.60	7.60	20.0	20.0	20.0
Simulated time (ns)	3.0	5.0	4.0	3.0	3.0	3.0
Equilibration period (ns)	1.5	3.5	2.5	1.5	1.5	1.5
Parameter	Micelle					
Label	mic-C8-pK_1-298	mic-pK_1-298	mic-pK_2-298	mic-bas-298	mic-64-bas-298	
Number of lipids	90	90	90	90	64	
Number of tail carbons	8	12	12	12	12	
Number of Na^+ ions	45	45	135	180	128	
Number of water-molecules	6208	6161	6071	6102	6102	
Atoms in total	19,974	20,193	19,923	20,016	19,522	
pH	p$K_1 \approx 2$	p$K_1 \approx 2$	p$K_2 \approx 7$	Basic	Basic	
T (K)	298	298	298	298	298	
Box shape	Trunc. octah.	Trunc. octah.	Trunc. octah.	Trunc. octah.	Trunc. octah.	
Pressure coupling	Isotropic	Isotropic	Isotropic	Isotropic	Isotropic	
Initial box length						
x (nm)	7.60	7.60	7.60	7.60	7.60	
y (nm)	7.60	7.60	7.60	7.60	7.60	
z (nm)	7.60	7.60	7.60	7.60	7.60	
Simulated time (ns)	3.0	3.0	3.0	8.0	3.0	
Equilibration period (ns)	1.5	1.5	1.5	1.5	1.5	

System equilibration

Initial velocities were taken from a Maxwell-Boltzmann distribution at the required temperature. Various properties were monitored as function of time to investigate equilibration and convergence. Equilibration could take as long as a few nanoseconds because of the slow diffusion of the charged particles under the influence of long-range Coulomb interactions. This is illustrated in Fig. 2.

All simulations have been carried out under the following identical conditions. Covalent bonds have been constrained using the SHAKE algorithm (Ryckaert et al. 1977) with a relative accuracy of 10^{-4}. For non-bonded interactions a twin-range cut-off scheme using 0.8 and 1.4 nm distance criteria was applied. Short-range forces were calculated at every time step of 2 fs, while intermediate-range forces were calculated every fifth step. A dielectric continuum with dielectric permittivity ϵ_2 equal to 54 (corresponding to SPC water) was assumed beyond the larger cut-off distance. Solute and solvent degrees of freedom were separately coupled to a temperature bath using the Berendsen thermostat (Berendsen et al. 1984) with a coupling time of 0.1 ps. The centre of mass motion was removed every 50 ps. The pressure was correspondingly coupled to one atmosphere with a coupling time of 0.5 ps and an isothermal compressibility $\kappa_T = 4.575 \times 10^{-6}$ (kJ mol^{-1} nm^{-3})$^{-1}$ was used as for mixed protein/water systems (van Gunsteren et al. 1996). System configurations were saved every picosecond for analysis.

Fig. 2a, b Various system properties as a function of time. The various systems are indicated with the abbreviations defined in Table 2. The total (*c*), kinetic (*a*) and potential energies (*d*) of the systems and electrostatic interaction energies between lipids and ions (*e*) and lipids and water interaction energies (*b*) are shown in the *top panels*. Room temperature (298 K) results are given as *solid black lines*, higher temperatures as *dark* (348 K) and *light* (398 K) *gray lines*. The *second panels* show the lengths of the axes of the computational boxes. The *third panels* show $-S_{CD}$ NMR order parameter values for the last CH_2 group in the lipid tails for the bilayer systems. For micelles, the average diameter of the micelle (in nanometers) is shown. The *lowest panels* show the average percentage of *trans* conformation seen in the terminal torsion angles of the lipid chains in the systems

Calculation of NMR $-S_{CD}$ order parameters

In NMR measurements aimed at obtaining order parameters, deuterated lipids are used and the measured directions are the CD bonds of the hydrocarbon tails. Since we use a united-atom model, the CD bond vectors are not directly available from the trajectory. Instead, other vectors were used. Considering the -CD_2- group at position n in the hydrocarbon tail, vectors orthogonal to the vector connecting the carbons at position n–1 and $n+1$ were considered, assuming that these would reflect the time motion of the CD bonds at carbon position n along the hydrocarbon tail. This technique has been introduced by Egberts and Berendsen (1988). For the nth -CH_2- united atom (C_n) we define $\boldsymbol{z}$ as the unit vector from C_{n-1} to C_{n+1}, $\boldsymbol{y}$ as the vector orthogonal to $\boldsymbol{z}$ in the plane through atoms C_{n-1}, C_n and C_{n+1}, and $\boldsymbol{x}$ as the vector orthogonal to $\boldsymbol{y}$ and $\boldsymbol{z}$. The calculation of the $-S_{CD}$ order parameter is done through Eq. 2, which takes into account the possible rotation of the tail, where θ_x and θ_y represent the angles between the orthogonal vectors $\boldsymbol{x}$ and $\boldsymbol{y}$ and the aggregate or bilayer normal:

$$1 - S_{CD} = -\left(\langle \cos^2 \theta_x \rangle + \frac{1}{2} \left(\langle \cos^2 \theta_y \rangle - 1 \right) \right) \qquad (2)$$

Calculation of hydrogen bond lifetimes

Hydrogen bonds were defined by a hydrogen-acceptor distance smaller than 0.25 nm and an acceptor-hydrogen-donor angle larger

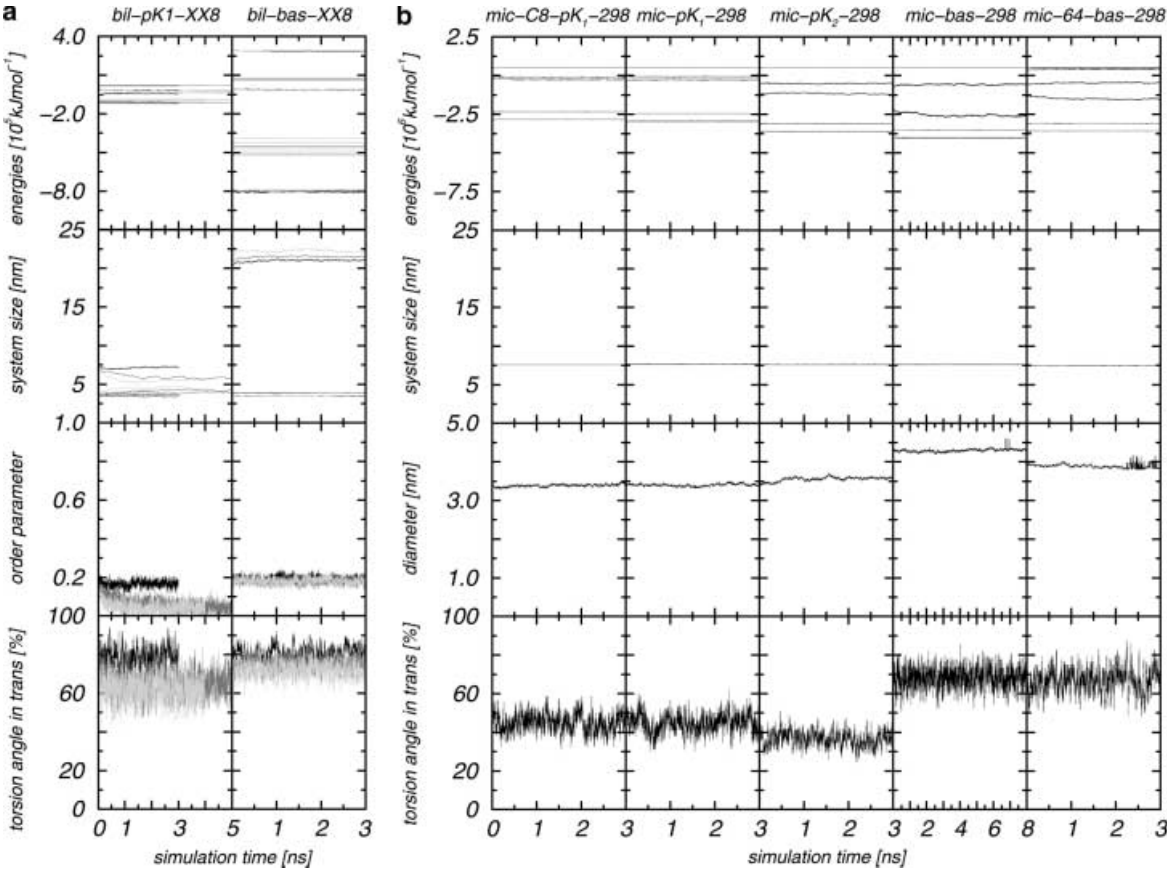

than 135° (van Gunsteren et al. 1996). The hydrogen bond lifetimes were calculated using a 2 ps time resolution.

Calculation of diffusion coefficients

Diffusion coefficients were calculated from the mean-square displacement of an atom using the Einstein relation.

Results and discussion

Figure 3 shows snapshots of simulated aggregates at the ends of the simulations. Under acidic conditions (pH≈2) the bilayers show increased disorder with increasing temperature. This is not observed under basic conditions (pH≥11). Under acidic conditions the micelles look rather spherical, under basic conditions more elongated (same pH as for bilayer systems). In some simulations, e.g. bil-pK_1-398 or mic-C8-pK_1-298, individual lipids escape from the bilayer or micelle into solution (the abbreviation bil-pK_1-398 stands for a bilayer system at pH = pK_1 at T = 398 K). Our nanosecond simulations are too short to obtain meaningful statistics regarding these processes.

Experimentally it has been found that the concentration of non-associated lipids in equilibrium with the vesicles is about 20 mM, or about one lipid within water for the acidic 128 lipid bilayer system at room temperature. At 298 K and at 348 K, no diffusion of an individual lipid from the aggregate to the bulk water is observed within a few nanoseconds. At 398 K, diffusion of 4–6 lipids into and from the solvent is observed. At room temperature in bil-pK_1-298 the lipids show an ordering with respect to the surface. This is obvious for the lower layer in Fig. 3 (angle of about 25° from bilayer normal). The upper layer shows a similar ordering, but in a different direction, which is not obvious from the picture. This behaviour has been observed for many single-tail lipid crystals (Bailey et al. 1950; Brown et al. 1955; Turner and Lingafelter 1955; von Sydow 1956; Schwartz et al. 1992; Bell and Rice 1993). The tilted ordering is not observed at high pH within bilayers (Fig. 3). Instead, a surface undulation is seen through the periodic box at room temperature, which disappears at higher temperatures.

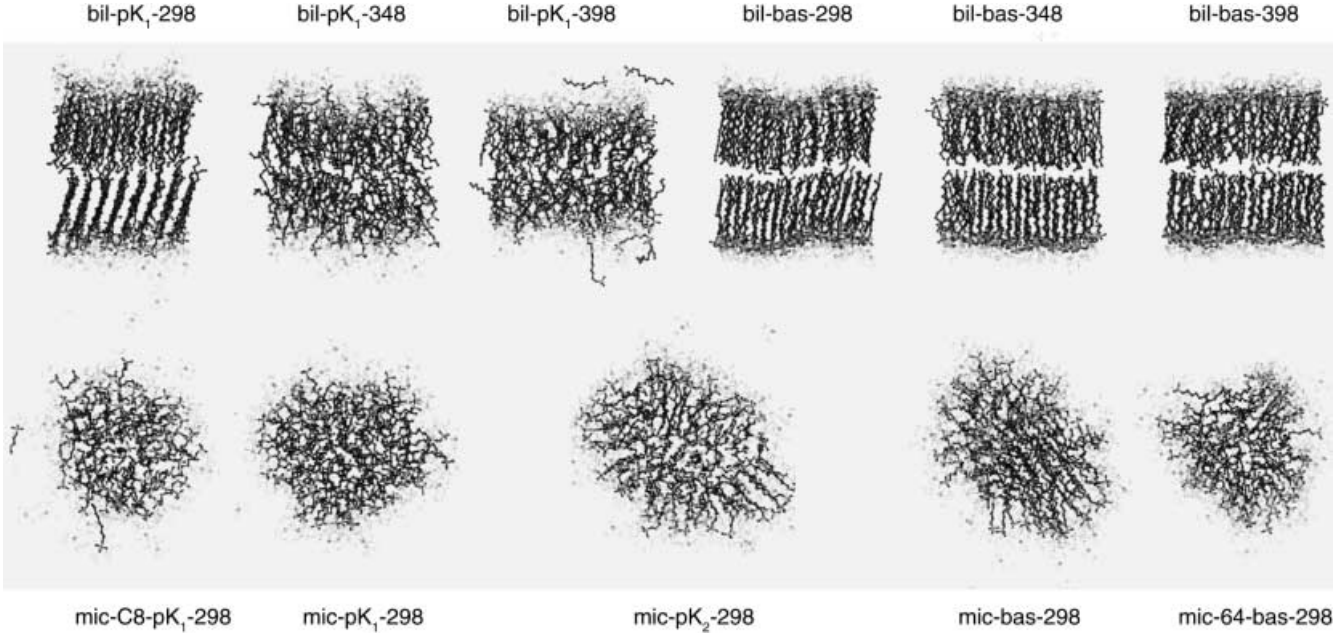

Fig. 3 *n*-Dodecyl phosphate structures obtained at the end of the lipid simulations. Lipid hydrocarbon tails appear in *black*, head groups in *intermediate gray shades*. Ions and solvent molecules close to them and to the lipids are shown in *light colours*. The display is laid out in five sections. *Upper left*: bilayer simulations at pK_1≈2 and at 298, 348 or 398 K. *Upper right*: bilayer simulations at basic pH = 11.2 and at 298, 348 or 398 K. *Lower left*: unstable micelles (90 lipids) at pK_1 and at 298 K with different carbon chain lengths (8 and 12 units). *Lower middle*: micelle (90 lipids) at pK_2≈7 and 298 K. *Lower right*: micelles (90 and 64 lipids) at basic pH and at 298 K. Thus, for example, mic-C8-pK_1-298 means the micellar system of 90 lipids with chain lengths of 8 carbons per lipid (default is always C_{12} = dodecyl phosphate) was built as the structure that reflects pH = pK_1 and has been simulated at T = 298 K. Any bilayer system of 128 lipids is abbreviated by bil correspondingly, and for micelles the labels of systems different from 90 lipids contain the aggregation number

Hydrogen bond lifetimes

Between lipid head groups of monoalkyl phosphoric acid and phosphate in the neutral and monoanionic protonation state, there are more potential hydrogen bonds than from these lipids to water molecules for systems at pK_1. For the bilayer bil-pK_1-298 at room temperature and acidic pH (Table 3), intermolecular hydrogen bonds of lipid head groups occur during 18% of the simulation time, whereas hydrogen bonds of head groups to water molecules are formed during 2% of the simulation time. For the same system the lifetime of

Table 3 Occurrence of hydrogen bonds (%) and average hydrogen bond lifetimes (ps). For both the bilayer and the micellar systems, lipid-lipid hydrogen bonds between the phosphate head groups and lipid-water hydrogen bonds between phosphate head groups and solvent molecules are given. Note that for structures simulated at basic pH, hydrogen bonds between lipid head groups cannot exist

Type of hydrogen bond	Bilayer simulation					
	bil-pK_1–298	bil-pK_1–348	bil-pK_1–398	bil-bas-298	bil-bas-348	bil-bas-398
Lipid-lipid						
Occurrence	17.6	5.7	1.3	–	–	–
Lifetime	8.6	5.0	3.3	–	–	–
Lipid-water						
Occurrence	2.0	0.8	0.4	5.1	1.2	0.6
Lifetime	13.3	7.5	4.2	4.4	1.2	0.7
	Micelle simulation					
	mic-C8-pK_1-298	mic-pK_1-298	mic-pK_2-298	mic-bas-298	mic-64-bas-298	
Lipid-lipid						
Occurrence	12.3	13.7	12.8	–	–	
Lifetime	16.3	8.8	14.4	–	–	
Lipid-water						
Occurrence	2.2	2.0	1.3	0.6	1.0	
Lifetime	25.6	24.1	12.1	4.6	4.7	

hydrogen bonds to water is longer than the lifetime of the hydrogen bonds between the lipids, 13 ps compared to 9 ps on average. The bilayer bil-bas-298 at high pH shows shorter lifetimes for hydrogen bonds to water of about 4 ps. Between lipids in the basic systems, no hydrogen bonds exist.

For micelles at acidic pH (mic-C8-pK_1-298 and mic-pK_1-298) the occurrence of hydrogen bonds is comparable for both systems, about 13% for hydrogen bonds between head groups and about 2% for hydrogen bonds of head groups to water. The lifetime of these hydrogen bonds is shorter (16 and 9 ps) between head groups than between head group and water (26 and 24 ps). The difference in tail lengths is, therefore, particularly reflected in the difference of lipid-lipid hydrogen-bonding lifetimes. Lipid to water hydrogen bonding has the same lifetime for the smaller *n*-octyl and the larger *n*-dodecyl phosphates. With increasing pH, the micelle at p$K_2 \approx$ pH = 7 (Tahara et al. 1969; Arakawa and Pethica 1980), mic-pK_2-298, shows similar hydrogen bonding characteristics as the simulated acidic micelle mic-pK_1-298 at p$K_1 = 2$ does for the intermolecular head-group hydrogen bonding, but hydrogen bonding of lipids to water (occurrence 1% and lifetime 12 ps) is reduced by a factor of 2. For micelles at basic pH (mic-bas-298 and mic-64-bas-298), almost no hydrogen bonds to water are observed (less than 1%) and their lifetime is shorter by a factor of 3. All this indicates that the lifetimes of hydrogen bonds to water in aggregates of *n*-dodecyl phosphoric acid and phosphates are clearly pH dependent.

The assumption that hydrogen bonding between lipid head groups is important to stabilize the lipid vesicles of *n*-dodecyl phosphoric acid and phosphates (bilayer patch in our model), as stated by Walde et al. (1997), is supported by these data. It seems that the mixing with water in the head-group region is low and contacts to water molecules are few. This intramembrane hydrogen-bonding network reflects a major effect of the acidic pH conditions and is not lost by the curvature in the micellar structure (comparing the bilayer and micelle at pK_1). On the other hand, the micelle structures at basic pH are purely stabilized through polar electrostatic interactions. Hydrogen bonding to water in the experimentally known micellar aggregates at basic pH lasts half as long as in bilayer membranes at acidic pH.

In the bilayer system bil-pK_1-298 the bulk water hydrogen bonds have a lifetime of 1.4 ps, which is shorter than for lipid to water (2 ps) and lipid-lipid (9 ps) hydrogen bonds.

Percentage *trans* of torsion angles along the lipid chains

For every carbohydrate tail the torsion angles θ along the lipid chain (starting at the head group) were calculated and the percentage *trans* population of the total population was determined. *Trans* was defined as $|\theta| > 120°$ and *gauche* as $|\theta| \leq 120°$. Figure 4 shows the averages for the different simulations.

The picture of the simulated structures for bilayers at different temperatures in Fig. 3 and the percentage *trans* in Fig. 4 show temperature dependence along the tails. The *trans* percentages can be compared to values measured for liquid *n*-alkanes for which about 2/3 of the corresponding torsion angles would be in the *trans* conformation at room temperature (Schuler and van Gunsteren 2000). Within the membrane, only the tail torsion angle might have the freedom to rotate as in a liquid. We note for acidic pH (bil-pK_1-298) this freedom is not given in the bilayer; at room temperature we find 7 out of 9 torsion angles to be over 90% in the *trans* conformation. At high pH and room temperature the

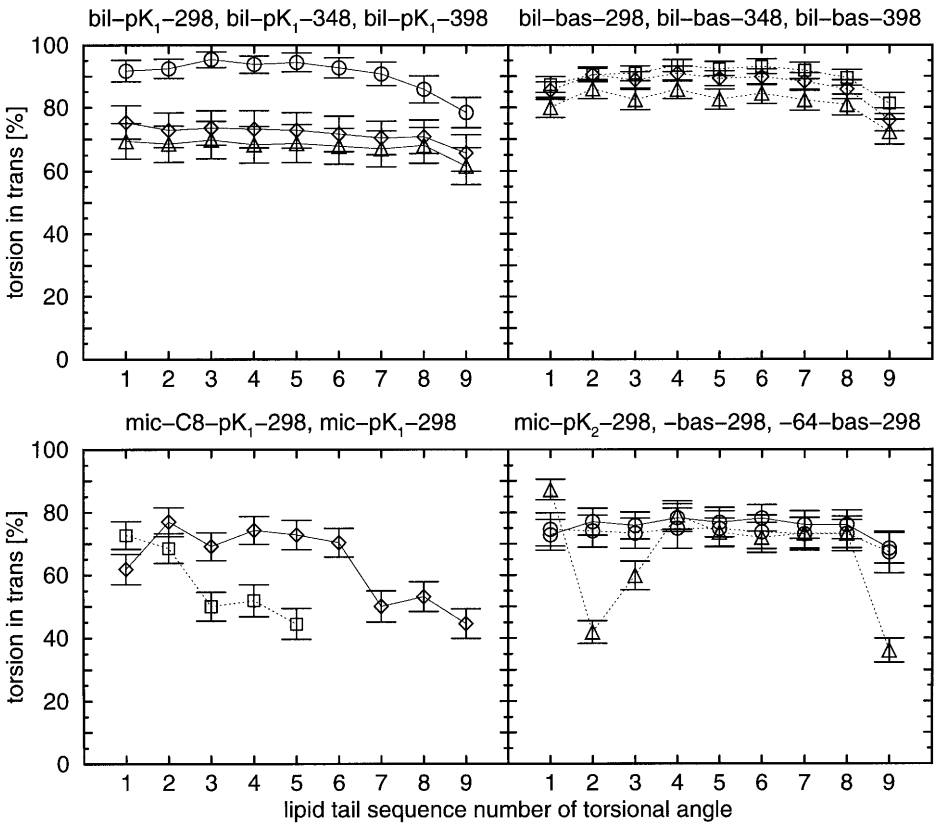

Fig. 4 Percentage of torsion angles in the *trans* conformation as a function of their positions in the lipid chains. *Upper left*: pK_1 bilayer, three temperatures: bil-298 (○), bil-348 (◇), bil-398 (△). *Upper right*: pH > 11 bilayer, three temperatures: bas-298 (○), bas-348 (◇), bas-398 (△). *Lower left*: pK_1 micelles at 298 K: mic-C8-pK_1-298 (□, dotted line), mic-pK_1-298 (◇). *Lower right*: pK_2 and pH > 11 micelles at 298 K: mic-pK_2-298 (△), mic-bas-298 (○, *solid line*), mic-64-bas-298 (○, *dotted line*)

structure (bil-bas-298) is less rigid than at low pH. Higher temperature simulations show a decreasing amount of *trans* conformations at acid pH (bil-pK_1-348, bil-pK_1-398); the membrane obviously melts and dissolves as seen in Fig. 3. At basic pH, there is instead only little liquefaction.

Micellar aggregates of 90 or 64 lipids at high pH conditions (mic-bas-298 and mic-64-bas-298) show less torsion angles in the *trans* conformation than bilayer membranes. The trend for tail torsion angles to adopt more *gauche* conformations is observed both in the micelles and in the bilayers. The smaller micellar aggregate shows less *trans* conformations. The experimentally nonexistent micelles (mic-pK_1-298, mic-pK_2-298) behave very differently. At pK_2, two distinct torsion angles seem to adopt the *gauche* conformation more strongly than the *trans*: a kind of screwed lipid structure with two *gauche* conformations is favoured. In the micellar aggregates at pK_1 the distribution of *trans* versus *gauche* conformations along the chain starting from the tail end is remarkable: both the pK_1 micelles with 90 lipids and different tail lengths (mic-C8-pK_1-298 and mic-pK_1-298) show the same trend for different torsion angles in sequence along the tails.

NMR $-S_{CD}$ order parameter

NMR measurements of $-S_{CD}$ order parameters provide a measure of the lipid tail ordering in bilayer membranes that are immobilized like in a planar Langmuir-Blodgett film (e.g. MacRitchie 1990). Deuterated hydrocarbons are synthesized for tail groups that are pure with respect to the unique deuterium (D) position along the tail. If the directions of the CD bonds are parallel, like they would occur in a frozen crystal, the order parameter value $-S_{CD}$ is one. If the distribution of directions is homogeneous, $-S_{CD}$ drops to zero. The order parameter $-S_{CD}$ in our simulations was calculated from the ensemble average of (Eq. 2) over time for the bilayers.

In Fig. 5, a comparison of bilayers at acidic pK_1 and basic pH shows that in the basic case only slightly more order is seen at room temperature. A temperature increase melts the acidic bilayer but not the basic one, which may be trapped in a metastable state. Since NMR order parameter measurements of *n*-dodecyl phosphate are not available, a comparison with experimental data for an *n*-dodecyl double-tail lipid, dilaurylphosphatidylcholine, obtained at room temperature from L_α-phase powder spectra (Douliez et al. 1995), is given in Fig. 5. It seems that the atoms near the end of the lipid tail in a double-tail lipid have more motional freedom than those of a single-tail lipid of the same length. Experiments for small deuterated *n*-alkyl chains that have been inserted or belong to lipid aggregates (Seelig and Niederberger 1974; Pope et al. 1984; Söderman et al. 1988) show a range of 0.18–0.24 for the NMR $-S_{CD}$ order parameter at position 1 next to the head group. A similar value of 0.20 is found in our simulation of an *n*-dodecyl phosphate bilayer.

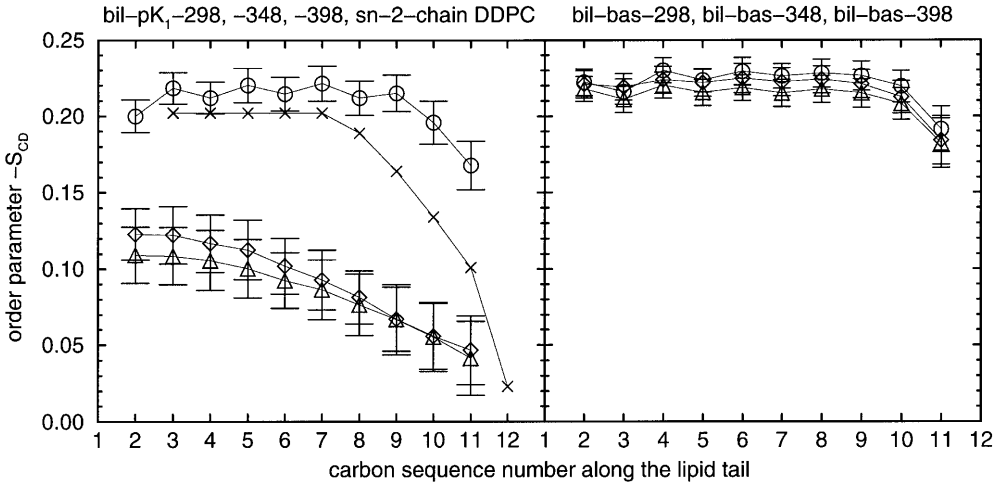

Fig. 5 NMR $-S_{CD}$ order parameter versus carbon numbers along the lipid chains. The $-S_{CD}$ NMR order parameters are displayed for all simulated bilayer systems of *n*-dodecyl phosphate. Both panels show the structures simulated at three different temperatures, 298 K (○), 348 K (◇) or 398 K (△), at pK_1≈2 *on the left* (experimental condition for vesicles of *n*-dodecyl phosphoric acid and *n*-dodecyl phosphate), at basic pH *on the right* (experimental condition for micelles of *n*-dodecyl phosphate). The experimental values for the deuterated sn2-chain of dilaurylphosphatidylcholine (Douliez et al. 1995) are shown for comparison (×)

Fig. 6 Distribution of atom types across bilayer membranes. The average distribution of different GROMOS96 atom types is compared (*OM*: double-bonded oxygen; *OA*: hydroxyl or ester oxygen; *OW*: water oxygen). The distributions have been normalized

Distribution of atom types: cross section for bilayers

The average distribution of particles (here distinguished by atom types) within the simulated system shows how close the different atoms come to each other. Figure 6 contains the atom distributions along the *z*-axis of the system (orthogonal to the bilayer plane) through the membrane, and shows all atom types present in the simulated system. Upon increasing the temperature of the acidic bilayer membrane (bil-pK_1-298, -348, -398) the peaks representing head-group atoms (OM, OA, P) move closer to each other, indicating that the membrane is getting thinner. In addition, the intermingling of the tails increases, because the distribution histograms of the CH_2

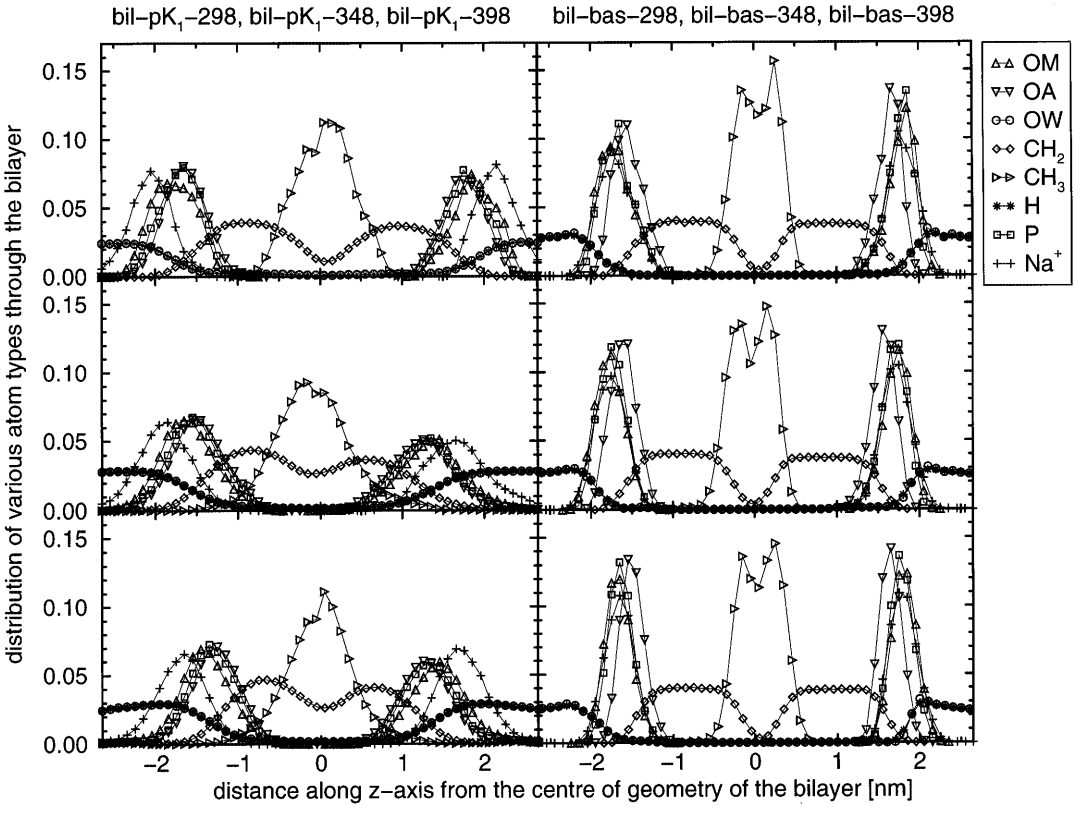

groups of the two layers which meet each other in the inner section of the bilayer start merging. No water atom types (OW, H) appear within the membrane, the water density is flat outside the bilayer and drops where head-group atoms appear. Statistically, water exchange through such a small system of 64 lipids in cross section is only a rare event. The simulation at high temperature, bil-pK_1-398, shows that few lipids are able to diffuse into the water within a simulation time of nanoseconds (Fig. 3). In a test simulation at 398 K, a water molecule was only once observed crossing the *n*-dodecyl phosphate lipid bilayer. For longer simulations and larger systems, such events may also be observed at lower temperature.

The basic bilayer (bil-bas-298, -348, -398) shows a gap between the two layers; the CH_3 atom density is reduced (Fig. 6). The CH_2 group distribution is more flat than at acidic pH and much closer contacts of ions (Na^+ atom type) to the head-group atoms (P, OM, OA atom types) are found. No water is found within the membrane. No significant change with temperature occurs in the distributions.

Distribution of atom types: radial distribution for micelles

Micelles very often adopt a spherical (spherical micelles) or cylindrical (rod-like micelles) geometry. Radial distributions for the different atom types are shown in Fig. 7. The micelles simulated at acidic pH (pK_1) differ mainly in size; the head-group peaks of P, OM and OA atom types for mic-C8-pK_1-298 appear at a lower distance than for mic-pK_1-298. The spread of the lipids through the computational box is wider in the former: for mic-C8-pK_1-298 a CH_3 united atom is present at a maximum distance of 4.5 nm from the centre of the micelle, whereas for mic-pK_1-298 this value is 3.3 nm. Both micellar structures at high pH (mic-bas-298, mic-64-bas-298), which only differ in the number of lipids and counterions, show different distributions. For 64 lipids there is a considerable overlap between ions (Na^+) and head-group atoms (P, OM, OA) and tail atoms (CH_2, CH_3). The sharper distributions for the large aggregates of 90 lipids at high pH (mic-bas-298) is much more comparable with the lipid aggregate of 90 lipids at neutral pH = pK_2 = 7 (mic-pK_2-298). Common to all micellar distributions is the appearance of tail-end atom types (CH_3) up to close to the head group (P, OM, OA) atom types, illustrating that lipids in micelles are able to expose their tails to the micellar surface. In three micellar systems (mic-C8-pK_1-298, mic-bas-298, mic-64-bas-298) we found lipid tail traces up to 4.5 nm. Experiments that provide the aggregation numbers for *n*-octyl phosphate (43 ± 5 lipids; Chevalier and Chachaty 1984) and *n*-dodecyl phosphate (90 lipids; Tahara et al. 1969) leave room for variation in the number of lipids in an aggregate. The number of lipids in the aggregate also varies in the simulation. Single lipids diffuse into the solvent and back into the micelle (mic-64-bas-298 and

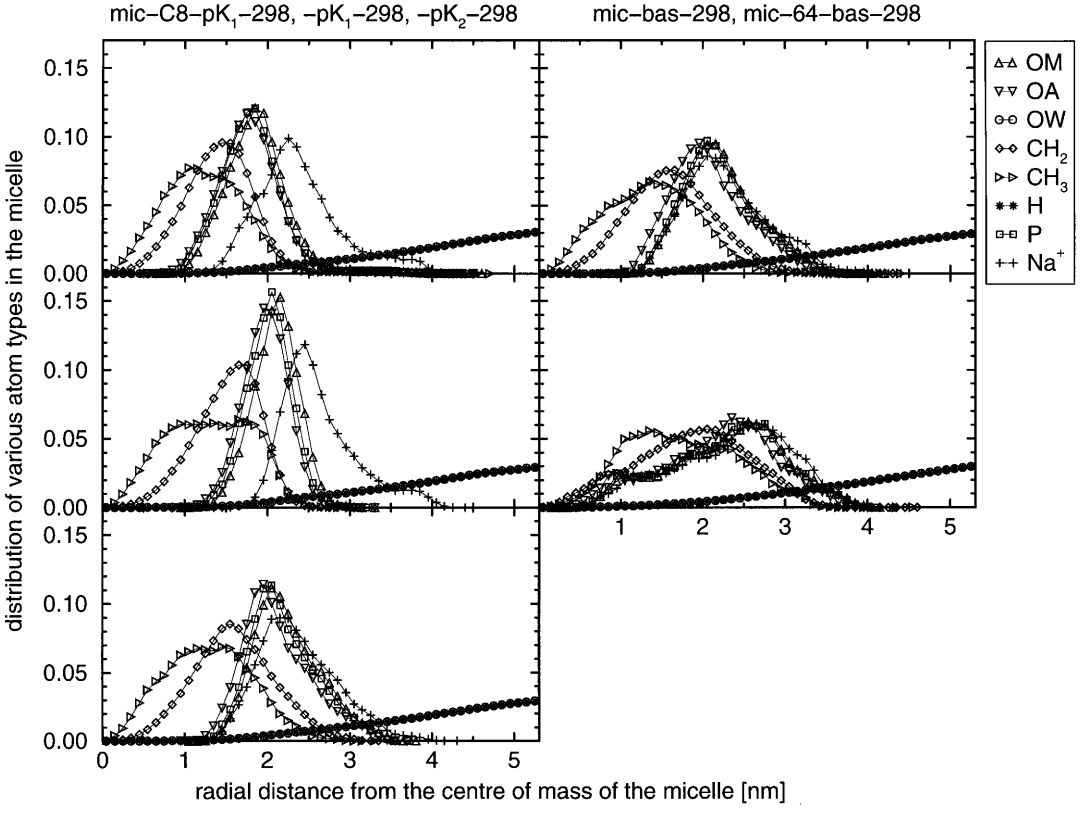

Fig. 7 Radial distribution of atom types from the centre of the micelles. The average distribution of different GROMOS96 atom types is compared (see caption of Fig. 6)

mic-bas-298) and the shorter tail lipid aggregate (mic-C8-pK_1-298) loses several aggregate members.

Diffusion coefficients

From the atom mean-square displacement, the diffusion coefficients for lipids (P atoms) and counterions (Na^+ atoms) were estimated (Fig. 8). The results are displayed in Table 4. Sodium counterions move faster than the lipids (phosphorus head-group atoms). For lipid diffusion we estimate 2×10^{-6} cm^2 s^{-1} for bilayer membranes of *n*-dodecyl phosphoric acid and phosphate (bil-pK_1-298), a value that increases with temperature. Not unexpectedly, both counterion and lipid diffusion decrease with decreasing acidity. Sodium ions are (according to Fig. 7) less surface bound at acidic micelles and this may explain the faster diffusion in comparison with the basic micelles or the acidic bilayer. Within the lipid bilayer at room temperature, lipids laterally diffuse faster than within micelles. In micellar aggregates at high pH (mic-bas-298), a factor of two difference between large (90) and small (64) aggregation numbers with 1×10^{-6} cm^2 s^{-1} and 2×10^{-6} cm^2 s^{-1} was found. The essential contribution to lipid diffusion in micelles might be the micelle rotation and diffusion and not the movement of the strongly interacting lipids themselves, since lipid diffusion of the larger micelle mic-bas-298 is slower than for the smaller micelle mic-64-bas-298. In general, experimentally determined diffusion coefficients for lipids in membranes are in the range 10^{-8} to 10^{-6} cm^2 s^{-1} (e.g. Essmann and Berkowitz 1999).

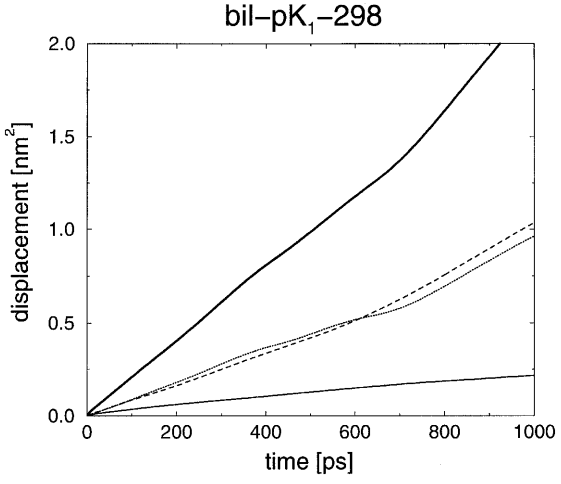

Fig. 8 Example of data calculated to estimate the diffusion coefficient. Measurements have been taken over 3 ns from a trajectory of the *n*-dodecyl phosphate bilayer at pK_1 and at 298 K which has been elongated from 3 to 6 ns. Of these, only the first nanosecond for the sodium counterions is shown. The *lower thin line* corresponds to the mean-square displacement orthogonal to the lipid bilayer membrane plane (*z* direction), whereas the *parallel dashed and dotted lines* represent the displacement in the orthogonal *x* and *y* directions lateral in the bilayer membrane plane. The *thick black line* represents the three-dimensional displacement. Its slope leads to a value of $D = 3.3\times10^{-6}$ cm^2 s^{-1} (see Table 4 for bil-pK_1-298)

Torsion angle dynamics

The internal dynamics of the lipid chains can be analysed in terms of torsion angle transitions between potential energy minima. The three potential energy wells of the X-CH_2-CH_2-Y torsion angle potential energy term in the force field are used to define the transitions. The transitions for every torsion angle along the lipid chains were counted and averaged over the number of molecules (Fig. 9).

With increasing temperature the frequency of transitions increases for both bilayer systems, bil-pK_1-298, -348, -398 and bil-bas-298, -348, -398. The increase is, however, more pronounced for the acidic bilayer system. In the case of the different micelles, at high pH (mic-bas-298, mic-64-bas-298) or at neutral pH (mic-pK_2-298) there is no difference in frequency of torsion angle transitions. The acidic micellar systems (mic-pK_1-298 and mic-C8-pK_1-298) show barely faster transitions.

Conclusions

The membrane and micellar aggregates of *n*-dodecyl phosphoric acid and *n*-dodecyl phosphate as set at the beginning of the simulations do not lose their integrity

Table 4 Diffusion coefficients (10^{-6} cm^2 s^{-1}) from mean-square displacement of atoms. The diffusion of phosphorus atoms is taken for the lipid diffusion within (lateral) or out of the membrane (bulk diffusion)

	Bilayer simulation					
	bil-pK_1-298	bil-pK_1-348	bil-pK_1-398	bil-bas-298	bil-bas-348	bil-bas-398
Na^+ ions	3.3	9.0	14.2	1.6	3.0	4.6
P bulk	2.1	3.6	5.3	1.1	2.0	2.8
P lateral	2.6	4.6	6.9	1.1	1.5	3.9
	Micelle simulation					
	mic-C8-pK_1-98	mic-pK_1-298	mic-pK_2-298	mic-bas-298	mic-64-bas-298	
Na^+ ions	8.7	7.7	4.3	2.1	4.2	
P bulk	1.9	1.2	2.5	1.0	2.2	

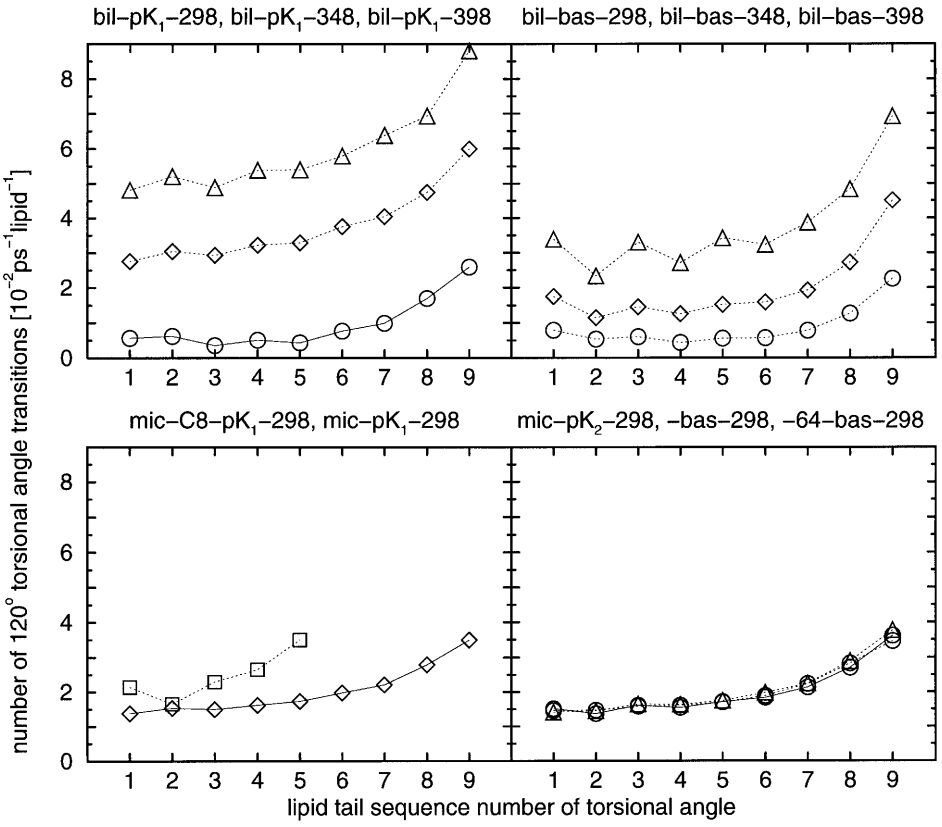

Fig. 9 Number of transitions between the three wells of the torsion angle per 100 ps as a function of the torsion angle sequence number along the lipid chains. *Upper left*: pK_1 bilayer, three temperatures: bil-pK_1-298 (○), bil-pK_1-348 (◇), bil-pK_1-398 (△). *Upper right*: pH > 11 bilayer, three temperatures: bil-bas-298 (○), bil-bas-348 (◇), bil-bas-398 (△). *Lower left*: pK_1 micelles at 298 K: mic-C8-pK_1-298 (□), mic-pK_1-298 (◇). *Lower right*: pK_2 and pH > 11 micelles at 298 K: mic-pK_2-298 (△), mic-bas-298 with 90 lipids (○, *solid line*), mic-64-bas-298 with 64 lipids (○, *dotted line*)

over a simulation time of 3–8 ns. Indeed, the head-group area that was roughly estimated to be 0.21 nm^2 for *n*-dodecyl phosphate bilayers (Eq. 1) was calculated to be 0.20 nm^2 in the simulation. A micelle of aggregation number 90 (mic-bas-298) seems to be more stable than a smaller one of aggregation number 64 (mic-64-bas-298), since the latter shows more diffusive character and tends to lose lipids more easily. This is in agreement with experiment.

The experimentally determined phase transition temperature T_m is about 276 K for the bilayer membrane system (Walde et al. 1997), which our simulation contradicts. At p$K_1 = 2$ and room temperature (298 K) the bilayer membrane looks as if in a so-called "gel phase" below the phase transition temperature (Fig. 3), but melts when heated up. The liquefaction of the micelle is observed through more transitions of torsion angles when the pH is lowered to pK_2 or pK_1. We assume this liquefaction to be indicative for a structural transition on the longer timescale. On the other hand, a bilayer structure of *n*-dodecyl phosphate that is simulated at high pH shows a ripple phase structure at room temperature (Fig. 3), but does not lose its integrity after transition towards a liquid crystalline phase when the temperature is raised. We see partial dissolution of a 90-member micellar aggregate of shorter lipids of *n*-octyl phosphate. All these observations from MD simulations show that the force field set 43A2 strikes the balance between experimentally and energetically favoured and unfavoured structures in most cases.

The bilayer structure at low pH shows the profile of *trans* torsion angles along lipid tails that one could expect for a stable bilayer system, and melts upon heating. We find a similar proportion of *trans* torsion angles along lipid tails for the high pH micelles, but not for other micelles. In agreement with experiments, it is concluded that high pH energetically favours micelles of *n*-dodecyl phosphates over bilayer membranes.

The simulations allow for predictions that cannot be verified, since measurements are not available:

1. We would expect the NMR $-S_{CD}$ order parameter of *n*-dodecyl phosphate bilayers at the plateau region to be close to 0.215 ± 0.01. For the tail methyl group at the end of the lipid chain the value would decrease to below 0.10.
2. Lipid-lipid hydrogen bonds seem to stabilize the bilayer, and their lifetimes cover a broad range with an average value of 9 ps.
3. If water molecules are hydrogen bonded to *n*-dodecyl phosphate bilayers, they are bound longer than at micellar surfaces, for about 13 ps compared to 5 ps on average, whereas water-water hydrogen bonds live much shorter: 1.5 ps.
4. We expect sodium counterion diffusion to be around $D = 3\times10^{-6}$ cm^2 s^{-1}, lipid diffusion within bilayers or micelles around 2×10^{-6} cm^2 s^{-1}. Lipids may diffuse faster within bilayers than in micelles, since their torsional dihedral conformations in micelles display a chain entanglement that might hinder a faster

diffusion process. For the experimental lipid aggregate number in micelles the lipids appear half as diffusive as for bilayers, but not for the smaller micelle aggregate, where diffusion was equally fast.

References

Ahlström P, Berendsen HJC (1993) A molecular dynamics study of lecithin monolayers. J Phys Chem 97:13691–13702

Arakawa J, Pethica BA (1980) Micellization in aqueous solutions of monoalkyl phosphate salts. J Colloid Interface Sci 75:441–450

Bailey AE, Hilditch TP, Longenecker HE, Markley KS (1950) Melting and solidification of fats. Wiley, New York

Bell KP, Rice SA (1993) A molecular-dynamics study of the structure of a long-chain amphiphile monolayer adsorbed on ice IH. J Chem Phys 99:4160–4167

Berendsen HJC, Postma JPM, Gunsteren WF van, Hermans J (1981) Interaction models for water in relation to protein hydration. In: Pullmann B (ed) Intermolecular forces. Reidel, Dordrecht, pp 331–342

Berendsen HJC, Postma JPM, Gunsteren WF van, DiNola A, Haak JR (1984) Molecular dynamics with coupling to an external bath. J Chem Phys 81:3684–3690

Blöchliger E, Blocher M, Walde P, Luisi PL (1998) Matrix effect in the size distribution of fatty acid vesicles. J Phys Chem B 102:10383–10390

Boggs JM (1987) Lipid intermolecular hydrogen-bonding: influence on structural organization and membrane function. Biochim Biophys Acta 906:353–404

Brown DA, Malkin T, Maliphant GK (1955) An X-ray examination of long-chain alkyl dihydrogen phosphates and dialkyl hydrogen phosphates and their sodium salts. J Sci Ind Res India 14:1584–1588

Buwalda RT, Wagenaar A, Engberts JFBN (1997) Synthesis and aggregation behavior of cyclic single- and double-tailed phosphate amphiphiles: a novel class of phosphate surfactants. Comparison with the aggregation behavior of sodium di-*n*-alkyl phosphates. Liebigs Ann-Recueil 1745–1753

Callaway MJ, Tildesley DJ, Quirke N (1996) Molecular dynamics simulation of a Langmuir-Blodgett patch. Mol Simulat 18:277–301

Chevalier Y, Chachaty C (1984) NMR investigation of the micellar properties of monoalkylphosphates. J Colloid Polym Sci 262:489–496

Damodaran KV, Merz KM (1994) A comparison of DMPC-based and DLPE-based lipid bilayers. Biophys J 66:1076–1087

Daura X, Mark AE, Gunsteren WF van (1998) Parametrization of aliphatic CHn united atoms of GROMOS96 force field. J Comput Chem 19:535–547

Deamer DW (1997) The first living systems: a bioenergetic perspective. Microbiol Mol Biol Rev 61:239–261

Douliez J, Léonard A, Dufourc EJ (1995) Restatement of order parameters in biomembranes: calculation of C-C bond order parameters from C-D quadrupolar splittings. Biophys J 68:1727–1739

Egberts E, Berendsen HJC (1988) Molecular dynamics simulation of a smectic liquid crystal with atomic detail. J Chem Phys 89:3718–3732

Egberts E, Marrink SJ, Berendsen HJC (1994) Molecular dynamics simulation of a phospholipid membrane. Eur Biophys J 22:423–436

Essmann U, Berkowitz ML (1999) Dynamical properties of phospholipid bilayers from computer simulation. Biophys J 76:2081–2089

Israelachvili J (1991) Intermolecular & surface forces, 2nd edn. Academic Press, London

Gunsteren WF van, Berendsen HJC (1990) Computer simulation of molecular dynamics: methodology, applications and perspectives in chemistry. Angew Chem Int Ed Engl 29:992–1023

Gunsteren WF van, Billeter SR, Eising AA, Hünenberger PH, Krüger P, Mark AE, Scott WRP, Tironi IG (1996) Biomolecular simulation, the GROMOS96 manual and user guide. Hochschulverlag an der ETH Zürich and BIOMOS, Groningen

Gunsteren WF van, Daura X, Mark AE (1998) The GROMOS force field. In: Schleyer P von R (ed) Encyclopedia of Computational Chemistry, vol 2. Wiley, New York, pp 1211–1216

Kuhn H, Rehage H (1997) Solvation and counterion-distribution of sodium octanoate micelles studied by molecular dynamics simulations. Ber Bunsenges Phys Chem Chem Phys 101:1493–1500

Larson RG (1997) Simulations of self-assembly. Curr Opin Colloid Interface Sci 2:361–364

Luisi PL (1998) About various definitions of life. Orig Life Evol Biosph 28:613–622

Luisi PL, Walde P, Oberholzer T (1999) Lipid vesicles as possible intermediates in the origin of life. Curr Opin Colloid Interface Sci 4:33–39

MacKerell AD (1995) Molecular dynamics simulation analysis of a sodium dodecyl sulfate micelle in aqueous solution: decreased fluidity of the micelle hydrocarbon interior. J Phys Chem 99:1846–1855

MacRitchie F (1990) Chemistry at interfaces. Academic Press, San Diego

Morigaki K, Dallavalle S, Walde P, Colonna S, Luisi PL (1997) Autopoietic self-reproduction of chiral fatty acid vesicles. J Am Chem Soc 119:292–301

Ourisson G, Nakatani Y (1994) The terpenoid theory of the origin of cellular life: the evolution of terpenoids to cholesterol. Chem Biol 1:11–23

Ourisson G, Nakatani Y (1995) The terpenoid theory of the origin of cellular life: the evolution of terpenoids to cholesterol. Chem Biol 2:631

Pope JM, Walker LW, Dubro D (1984) On the ordering of *n*-alkane and *n*-alcohol solutes in phospholipid bilayer model membrane systems. Chem Phys Lipids 35:259–277

Ravoo BJ, Engberts JFBN (1994) Single-tail phosphates containing branched alkyl chains: synthesis and aggregation in water of a novel class of vesicle-forming surfactants. Langmuir 10:1735–1740

Ryckaert JP, Ciccotti G, Berendsen HJC (1977) Numerical integration of the cartesian equations of motion of a system with constraints: molecular dynamics of *n*-alkanes. J Comput Phys 23:327–341

Schuler LD, Gunsteren WF van (2000) On the choice of dihedral angle potential energy functions for *n*-alkanes. Mol Simulat 25:301–319

Schwartz DK, Schlossman ML, Pershan PS (1992) Reentrant appearance of phases in a relaxed Langmuir monolayer of tetracosanoid acid as determined by X-ray scattering. J Chem Phys 96:2356–2370

Scott WRP, Hünenberger PH, Tironi IG, Mark AE, Billeter SR, Fennen J, Torda AE, Huber T, Krüger P, Gunsteren WF van (1999) The GROMOS biomolecular simulation program package. J Phys Chem A 103:3596–3607

Seelig J, Niederberger W (1974) Deuterium labeled lipids as structural probes in liquid crystalline bilayers. J Am Chem Soc 96:2069–2072

Söderman O, Carlström G, Olsson U, Wong TC (1988) Nuclear magnetic resonance relaxation in micelles. J Chem Soc Faraday Trans 84:4475–4486

Sydow E von (1956) The normal fatty acids in solid state. A crystal structure investigation. Ark Kemi 9:231–231

Tahara T, Satake I, Matuura R (1969) The micellar properties of disodium monoalkyl phosphates in aqueous solutions. Bull Chem Soc Jpn 42:1201–1205

Tieleman P, Berendsen HJC (1996) Molecular dynamics simulations of a fully hydrated dipalmitoylphosphatidylcholine bilayer with different macroscopic boundary conditions and parameters. J Chem Phys 105:4871–4880

Tieleman DP, Marrink SJ, Berendsen HJC (1997) A computer perspective of membranes: molecular dynamics studies of lipid bilayer systems. Biochim Biophys Acta 1331:235–270

Tobias DJ, Klein ML (1996) Molecular dynamics simulation of a calcium carbonate calcium sulfonate reverse micelle. J Chem Phys 100:6637–6648

Turner JD, Lingafelter EC (1955) The X-ray crystallography of the *n*-aliphatic amides. Acta Crystallogr 4:104

Wagenaar A, Rupert L, Engberts JFBN, Hoekstra D (1989) Synthesis and vesicle formation of identical-chain and mixed-chain di-*n*-alkyl phosphate amphiphiles. J Org Chem 54:2638–2642

Walde P, Wick R, Fresta M, Mangone A, Luisi PL (1994) Autopoeitic self-reproduction of fatty-acid vesicles. J Am Chem Soc 116:11649–11654

Walde P, Wessicken M, Rädler U, Berclaz N, Conde-Frieboes K, Luisi PL (1997) Preparation and characterization of vesicles from mono-*n*-alkyl phosphates and phosphonates. J Phys Chem B 101:7390–7397

Yoneya M, Berendsen HJC (1994) Molecular dynamics simulation of chiral nematic liquid crystals. J Phys Soc Jpn 63:1025–1030

Zhang SC, Ouyang ZC (1999) Undulation modes in bilayer membranes. Acta Phys Sinica Overseas Ed 8:321–325